

Strain Effects on Hole Current in Silicon Nanowire FETs

Hideki Minari*, Tatsuro Kitayama, Masahiro Yamamoto, and Nobuya Mori*

Division of Electrical, Electronic and Information Engineering, Graduate School of Engineering, Osaka University,
Suita, Osaka 565-0871, Japan

*CREST, Japan Science and Technology Agency, Chiyoda, Tokyo 102-0075, Japan

Email: minari@si.eei.eng.osaka-u.ac.jp

Abstract—Hole transport simulation based on the nonequilibrium Green's function and tight-binding formalism has been performed for strained Si nanowire FETs with a diameter of 1.5 nm and 2.5 nm. Simulation results show that for Si nanowire FETs with a diameter of 2.5 nm, the compressive strain enhances the ballistic hole current, while the tensile strain gives opposite results. For Si nanowire FETs with a diameter of 1.5 nm, the ballistic hole current hardly depends on the strain magnitude.

I. INTRODUCTION

Nanowire (NW) FETs are considered to be one of the most promising device structures that provide effective gate control even at the nanoscale [1]. For the bulk MOSFETs, strained Si technology has been widely introduced to enhance the device performance [2]. For p-type NW FETs, confinement-induced mixing of the heavy-hole and the light-hole states [3] makes the subband dispersion quite non-parabolic and anisotropic [4], [5]. It is thus unclear whether the strain leads to superior device characteristics in p-type NW FETs.

In the present study, we investigate strain effects in ultra-small p-type Si NW FETs. We calculate the ballistic hole current in Si NW FETs with a diameter of $D = 1.5$ nm and 2.5 nm using atomistic nonequilibrium Green's function (NEGF) formalism combined with an empirical tight-binding (TB) approximation. The NEGF method [6]–[8] allows us to perform quantum transport simulation in ultrasmall devices. By combining the NEGF method with a TB method [9], [10], we achieve quantum-mechanical computations including full-band structures [11]–[13].

This paper is organized as follows: The device structures and the simulation method are described in Section II. Simulation results on a thicker nanowire of $D = 2.5$ nm are presented and discussed in Section III-A. NW diameter dependence is then presented in Section III-B. A summary is given in Section IV.

II. SIMULATION METHOD

We consider p-type gate-all-around Si NW FETs with a gate-length of 10 nm and SiO_2 -thickness of 1 nm (see Fig. 1). The diameter of the NW is $D = 1.5$ nm or 2.5 nm. The current flows along the [100]-direction (x -direction). The doping concentration in the source and drain regions, each of which is 7.5 nm long, is $N_A = 1 \times 10^{20} \text{ cm}^{-3}$. We simulate three types of devices with compressive strain (sample C), with tensile

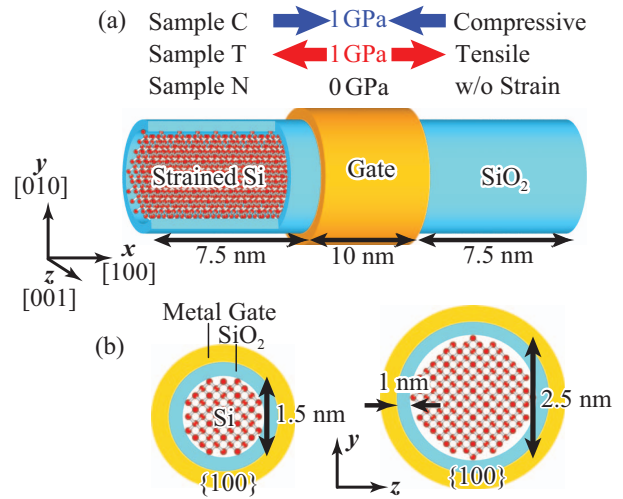


Fig. 1. (a) Schematic of a p-type strained Si NW FET structure. Uniaxial stress is applied along the [100]-direction (x -direction). (b) Cross sectional view of the Si NW FETs.

strain (sample T), and without strain (sample N). For strained Si channels, 1 GPa of uniaxial stress is applied along the x -direction.

We take into account the full-band structure within an empirical sp^3s^* nearest-neighbor TB approximation [14] and calculate ballistic hole current using the NEGF method. The sp^3s^* TB approximation includes five orbitals without the spin-orbit coupling. Strain effects are included by scaling the TB matrix elements with respect to the bond-length changes. The dependence of the two-center integral $ij\kappa$ on bond length is considered using the Harrison's d^{-2} law [15],

$$ij\kappa(d) = ij\kappa(d_0) \left(\frac{d_0}{d} \right)^{-2}. \quad (1)$$

Here d (d_0) is the strained (unstrained) interatomic distance. We use a macroscopic elastic theory [16] to evaluate the lattice constants of strained Si. We treated the Si/ SiO_2 interfaces with the H termination model [17] to eliminate the artificial surface states in the energy region of interest. In the present study, we neglect scattering and assume ballistic transport. The potential profiles are obtained through a self-consistent solution of three-dimensional Poisson and NEGF equations.

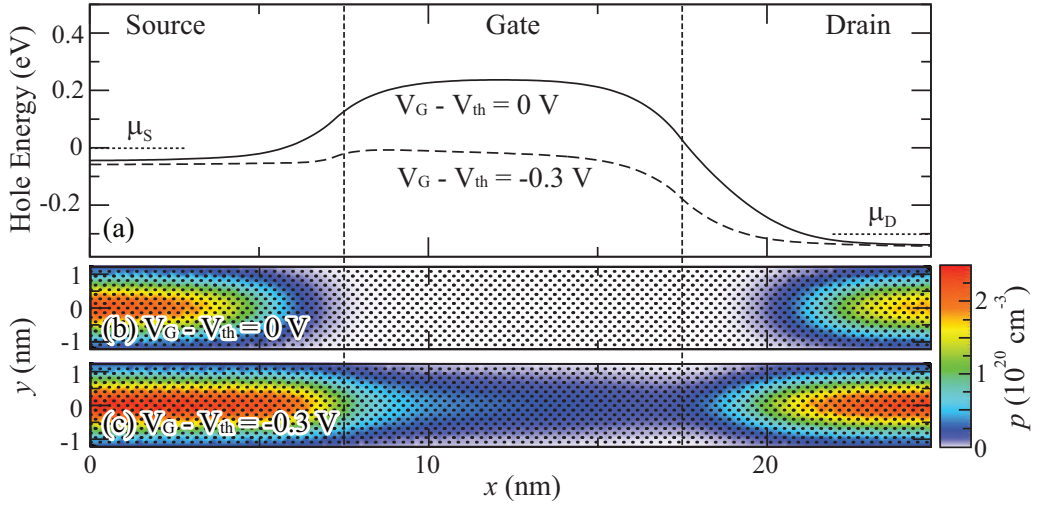


Fig. 2. (a) Potential profiles of the sample N with $D = 2.5$ nm at $V_D = 0.3$ V and $T = 300$ K for $V_G - V_{th} = 0$ V (solid line) and $V_G - V_{th} = -0.3$ V (dashed line). Dotted lines show the Fermi levels in the source (μ_S) and drain (μ_D) regions. Corresponding two-dimensional hole density profiles for (b) $V_G - V_{th} = 0$ V and (c) $V_G - V_{th} = -0.3$ V. Black dots represent the Si atomic positions.

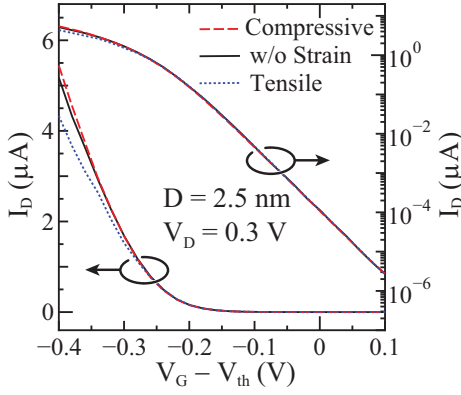


Fig. 3. Drain-current–gate-voltage characteristics of the devices with $D = 2.5$ nm at $V_D = 0.3$ V. Solid line shows the results for the sample N, dashed line for the sample C, and dotted line for the sample T.

III. RESULTS AND DISCUSSION

A. Strain Effects

We first discuss strain effects on on-current in the thicker NW FETs with $D = 2.5$ nm. Figure 2(a) shows the potential profiles of the sample N with $D = 2.5$ nm at $V_D = 0.3$ V and $T = 300$ K for $V_G - V_{th} = 0$ V and $V_G - V_{th} = -0.3$ V. The threshold voltage V_{th} is defined as the gate voltage V_G when the drain current is 1×10^{-4} μA. Figures 2(b) and 2(c) show the corresponding two-dimensional hole density profiles for $V_G - V_{th} = 0$ V and $V_G - V_{th} = -0.3$ V, respectively. Black dots represent the Si atomic positions. We considered 5,704 atoms in the calculation domain.

Figure 3 shows transfer characteristics of the devices with $D = 2.5$ nm at $V_D = 0.3$ V. The subthreshold swings are 62 mV/dec for the sample C, 62 mV/dec for the sample N, and 61 mV/dec for the sample T, showing that these devices maintain a good gate control with an almost ideal subthreshold

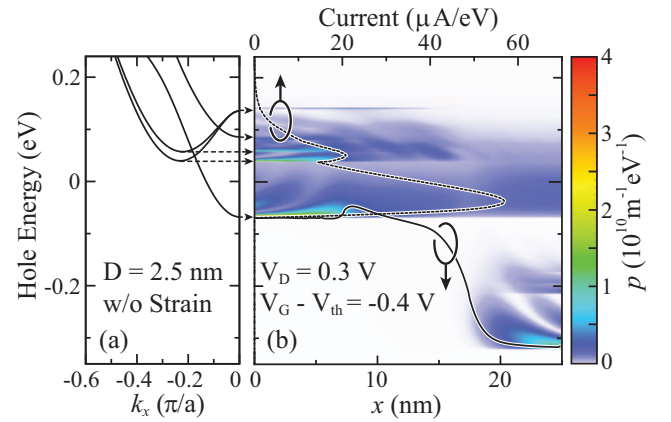


Fig. 4. (a) Subband dispersion in the source lead and (b) the local hole density spectrum of the sample N with $D = 2.5$ nm at $V_D = 0.3$ V and $V_G - V_{th} = -0.4$ V. Solid line shows the potential profile and dotted line the current spectrum.

swing. The drain current of the sample C is 6 % higher than that of the sample N at $V_G - V_{th} = -0.4$ V, while the drain current of the sample T is 16 % lower than that of the sample N. These features can be understood by considering the strain-induced energy shift of the subband levels.

Figure 4(a) shows the subband dispersion of the sample N with $D = 2.5$ nm in the source lead. The energy zero is chosen to be the Fermi level at the source contact. The energy minimum of the lowest subband locates at $k_x = 0$, while those of some higher subbands locate at off $k_x = 0$ (we call those subbands "off-valley subbands" hereinafter). Figure 4(b) shows the local hole density and current spectrum at $V_D = 0.3$ V and $V_G - V_{th} = -0.4$ V. Both the lowest subband and the off-valley subbands contribute to the drain current.

Figure 5 shows the subband dispersion of the devices

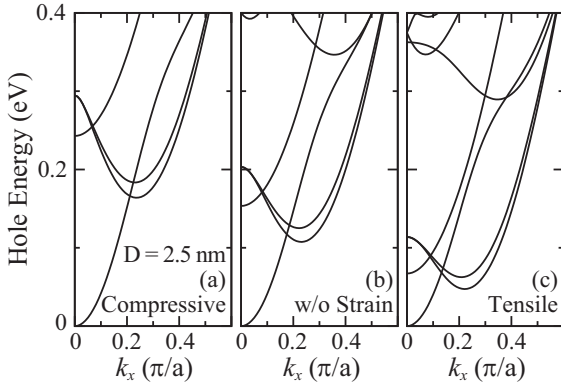


Fig. 5. Subband structures of the Si NWs with $D = 2.5$ nm under (a) compressive strain, (b) no strain, and (c) tensile strain.

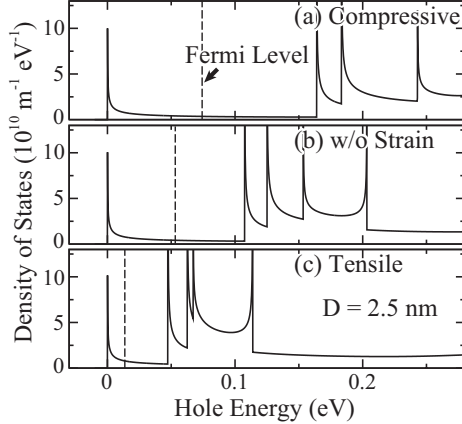


Fig. 6. Density of states of the Si NWs with $D = 2.5$ nm under (a) compressive strain, (b) no strain, and (c) tensile strain. Dashed lines show the Fermi levels for the doping concentration of $1 \times 10^{20} \text{ cm}^{-3}$.

with $D = 2.5$ nm. The energy zero is chosen to be the lowest subband level. Under compressive strain, the off-valley subband levels become higher than those of the device without strain. On the other hand, under tensile strain, the off-valley subband levels become lower than those of the device without strain. Figure 6 shows the density of states of the devices with $D = 2.5$ nm. The dashed lines show the Fermi levels for the doping concentration of $N_A = 1 \times 10^{20} \text{ cm}^{-3}$. For the compressive strain, the Fermi level moves upward in energy because of the higher off-valley subband levels under compressive strain. The off-valley population then becomes smaller for the compressive strain. Since the effective masses of the off-valley subbands are heavier compared to the lowest subband, the average effective mass contributing to the current becomes lighter by the compressive strain. As a result, the hole current is enhanced under compressive strain. On the other hand, under tensile strain, the population of the off-valley subbands becomes larger. Therefore, the average effective mass contributing to the current becomes heavier and the hole current is reduced by the tensile strain.

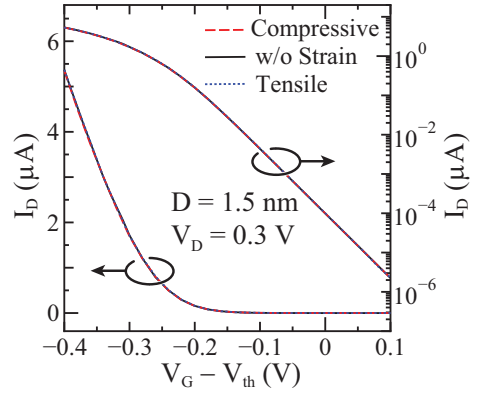


Fig. 7. The same as Fig. 3 but for the devices with $D = 1.5$ nm.

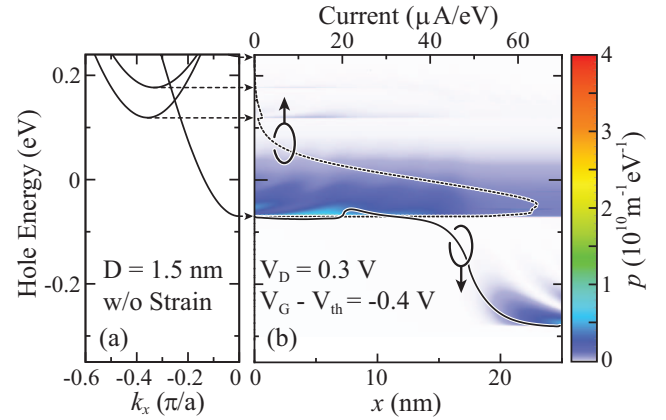


Fig. 8. Same as Fig. 4 but for the sample N with $D = 1.5$ nm.

B. NW Diameter Dependence

Figure 7 shows transfer characteristics of the thinner Si NW FETs with $D = 1.5$ nm at $V_D = 0.3$ V. Note that the doping concentration (per unit volume) is chosen to be the same as in the thicker NW FETs with $D = 2.5$ nm; i.e. $N_A = 1 \times 10^{20} \text{ cm}^{-3}$. The subthreshold swings are 60 mV/dec for the sample C, 61 mV/dec for the sample N, and 61 mV/dec for the sample T. We find that the drain current is hardly affected by the strain, which can be understood again by considering the off-valley subband levels.

Figure 8 shows the subband dispersion, local hole density, and current spectrum of the sample N with $D = 1.5$ nm at $V_D = 0.3$ V and $V_G - V_{th} = -0.4$ V. For the thinner NW FETs, holes are mainly occupied in the lowest subband and the off-valley holes do not contribute to the current. This results in the drain current being independent of the strain. Note that there is very weak dependence of the lowest-subband effective mass on the strain.

The fact that holes are mainly occupied in the lowest subband can be explained in terms of the hole subband structure and small hole line density. Figure 9 shows the subband dispersion of the devices with $D = 1.5$ nm. The energy separations between the lowest subband level E_0 and the off-valley subband level E_{off} are larger compared to the

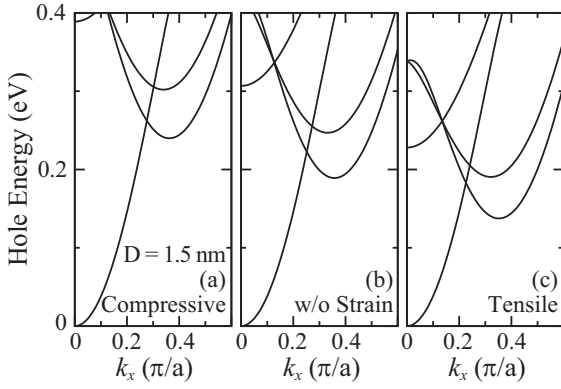


Fig. 9. The same as Fig. 5 but for the Si NWs with $D = 1.5$ nm.

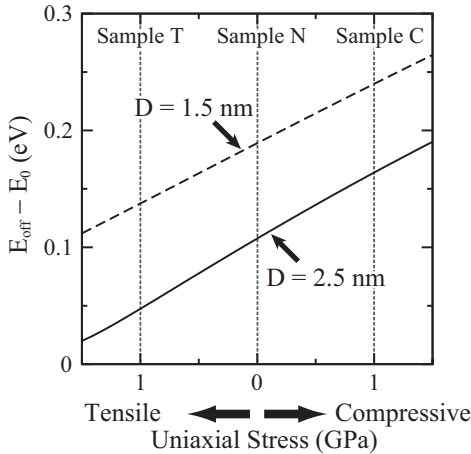


Fig. 10. Stress dependence of the energy separation between the lowest subband level E_0 and the off-valley subband level E_{off} . Solid line shows the result for the Si NWs with $D = 2.5$ nm and dashed line for the Si NWs with $D = 1.5$ nm.

thicker NW devices. The energy shift of the E_{off} due to the strain is almost equal to that of the thicker NWs (see Fig. 10). Since we compare the thicker NW and the thinner NW on the condition that the hole volume densities, h_{3D} , are the same in both device structures. As a result, the hole line density, $h_{1D} = \pi(D/2)^2 h_{3D}$, of the thinner NWs become smaller than that of thicker NWs. Because of this smallness of the hole line density and the larger off-valley separation, the lowest subband can accommodate all the holes for the thinner NWs. This can be readily seen in Fig. 11 where we plot the density of states of the thinner NWs together with the Fermi level position.

IV. CONCLUSION

In order to investigate the strain effects in ultrasmall p-type Si NW FETs, hole transport simulation based on the NEGF and TB formalism has been performed for strained Si NW FETs with a diameter of 1.5 nm and 2.5 nm. We found that for the thicker NW FETs with a diameter of 2.5 nm, the compressive strain enhances the ballistic hole current, while the tensile strain gives opposite results. We also found that for the thinner NW FETs with a diameter of 1.5 nm, the ballistic

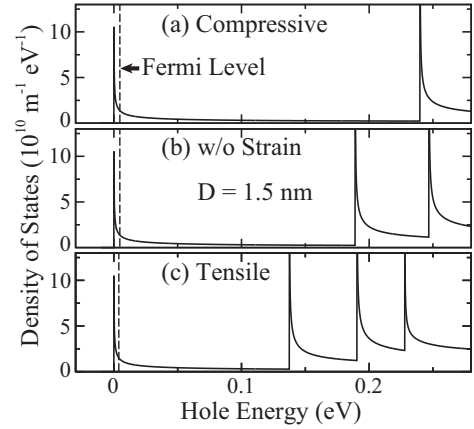


Fig. 11. Same as Fig. 6 but for the Si NWs with $D = 1.5$ nm.

hole current hardly depends on the strain magnitude. These features can be understood by considering the strain-induced energy shift of the subband levels.

REFERENCES

- [1] N. Singh, F.Y. Lim, W.W. Fang, S.C. Rustagi, L.K. Bera, A. Agarwal, C.H. Tung, K.M. Hoe, S.R. Omampuliyur, D. Tripathi, A.O. Abeyeye, G.Q. Lo, N. Balasubramanian, and D.L. Kwong, "Ultra-Narrow Silicon Nanowire Gate-All-Around CMOS Devices: Impact of Diameter, Channel-Orientation and Low Temperature on Device Performance", *IEDM Tech. Digest*, 2006.
- [2] S. Takagi, T. Mizuno, T. Tezuka, N. Sugiyama, S. Nakahara, T. Numata, J. Koga, and K. Uchida, "Sub-band structure engineering for advanced CMOS channels", *Solid-State Electron.*, vol. 49, 684, 2005.
- [3] C. Weisbuch and B. Vinter, *Quantum Semiconductor Structures: Fundamentals and Applications*, Academic Press, New York, 1991, p. 11.
- [4] H. Minari and N. Mori, "Hole Transport Mechanism in Silicon and Germanium Nanowire Field Effect Transistors", *Jpn. J. Appl. Phys.*, vol. 49, 04DN04, 2010.
- [5] G. Klimeck, R.C. Bowen, and T.B. Boykin, "Strong wavevector dependence of hole transport in heterostructures", *Superlattices Microstruct.*, vol. 29, 187, 2001.
- [6] S. Datta, *Electronic Transport in Mesoscopic Systems*, Cambridge University Press, Cambridge, U.K., 1995, p. 293.
- [7] H. Haug and A.-P. Jauho, *Quantum Kinetics in Transport and Optics of Semiconductors*, Springer, Berlin, 1996, p. 35.
- [8] M. Lundstrom and J. Guo, *Nanoscale Transistors: Device Physics, Modeling, and Simulation*, Springer, New York, 2006, p. 21.
- [9] J.C. Slater and G.F. Koster, "Simplified LCAO Method for the Periodic Potential Problem", *Phys. Rev.*, vol. 94, 1498, 1954.
- [10] P.O. Löwdin, "On the Non-Orthogonality Problem Connected with the Use of Atomic Wave Functions in the Theory of Molecules and Crystals", *J. Chem. Phys.*, vol. 18, 365, 1950.
- [11] A. Di Carlo, "Tight-binding methods for transport and optical properties in realistic nanostructures", *Physica B*, vol. 314, 211, 2002.
- [12] A. Pecchia and A. Di Carlo, "Atomistic theory of transport in organic and inorganic nanostructures", *Rep. Prog. Phys.*, vol. 67, 1497, 2004.
- [13] C. Rivas and R. Lake, "Non-equilibrium Green function implementation of boundary conditions for full band simulations of substrate-nanowire structures", *Phys. Status Solidi B*, vol. 239, 94, 2003.
- [14] G. Klimeck, R.C. Bowen, T.B. Boykin, C. Salazar-Lazaro, T.A. Cwik, A. Stoica, "Si tight-binding parameters from genetic algorithm fitting", *Superlattice Microstruct.*, vol. 27, 77, 2000.
- [15] W.A. Harrison, *Electronic Structure and The Properties of Solids*, Dover, New York, 1989, p. 48.
- [16] C.G. Van de Walle, "Band lineups and deformation potentials in the model-solid theory", *Phys. Rev. B*, vol. 39, 1871, 1989.
- [17] S. Lee, F. Oya, P. von Allmen, and G. Klimeck, "Boundary conditions for the electronic structure of finite-extent embedded semiconductor nanostructures", *Phys. Rev. B*, vol. 69, 045316, 2004.